First Demonstration of Surface Currents Imaged by Hybrid Along- and Cross-Track Interferometric SAR

Robert Siegmund, Mingquan Bao, Susanne Lehner, *Member, IEEE*, and Roberto Mayerle

***Abstract*—This paper is concerned with the simultaneous measurement of terrain heights and currents using an airborne interferometric synthetic aperture radar (INSAR). For the first time, a hybrid two-antenna INSAR system with both along- and across-track baseline components is used to measure high-resolution digital elevation maps (DEMs) and current fields in a Wadden sea area. Coastal applications like the monitoring of sediment transport or the numerical modeling of morphodynamic processes require measurements of topography and currents. Classical *in situ* measurements of these parameters are both expensive and time consuming, or even impossible if higher spatial resolution is required. Pure along-track interferometers (ATIs) have demonstrated their ability to provide information on ocean currents, while across-track interferometric systems (XTIs) have been successfully used to measure DEMs. In this paper, a hybrid system with both ATI and XTI components is used to acquire synoptic measurement for the first time. An experiment with an airborne system taking data over a Wadden sea area is presented demonstrating the potential of the technique. A geometrical model is developed for the interferometric phase of hybrid INSAR systems. This model combines ATI and XTI techniques using a baseline that spans between two antennas consisting of along-track and across-track components. In this model, both the effect of topography and the radial velocity of the water surface enter into the resulting interferometric phase. To separate both components, the system takes data of the respective scene flying two or more tracks with different flight directions, e.g., antiparallel tracks. This approach leads to a set of linear equations that has a unique solution for the along- and cross-track phase. Finally, an additional phase bias has to be considered due to the radial velocity and the influence of squint. This is caused by a misregistration effect between both antennas, which is related to cross-track imaging of surface motion. The new INSAR technique is tested with data acquired during a campaign in February 1997 over the Weser Estuary at the German coast. The airborne INSAR system AeS-1 was used. The interferometer configuration consists of two SAR antennas separated by a mixed along-track and cross-track baseline. Two datasets acquired on antiparallel tracks are used. The calculated velocities were compared with a hydrodynamic model operated by the Federal Waterway Engineering and Research Establishment. The experimental results agree well with the numerical model. In particular, the mean velocity of 0.7 ms^{-1} matches in both datasets. Deviations in the fine-scale structure of the current field are discussed. Topographic analysis and validation are performed in a separate investigation. The impact of surface gravity waves and wind drift, which are known to cause significant artifacts in the ATI phase under certain circumstances, is discussed.**

Manuscript received December 11, 2002; revised June 3, 2003.

R. Siegmund is with the Intermap Technologies GmbH, DLR, D-82234 Oberpfaffenhofen, Germany (e-mail: Robert.Siegmund@intermap.ca).

M. Bao and S. Lehner are with the German Aerospace Research Center (DLR), D-82234 Oberpfaffenhofen, Germany.

R. Mayerle is with the University of Kiel, D-24098 Kiel, Germany.

Digital Object Identifier 10.1109/TGRS.2003.817816

***Index Terms*—Airborne radar, along/cross-track interferometry, coastal application, mixed baseline, ocean surface currents.**

I. Introduction

INTERFEROMETRIC synthetic aperture radar (INSAR) is known to be a useful tool for measuring terrain height and ocean surface currents. Usually, the INSAR system employs two antennas that are spatially separated by a fixed distance either along or across the flight direction of the platform. Those INSAR systems are called along-track interferometric SAR (ATI) or cross-track interferometric SAR (XTI). In order to combine both techniques, a first analysis of a joint INSAR measurement of terrain height and surface currents with two antennas is presented. The method is tested with experimental data acquired over the Weser Estuary that is part of the Wadden Sea area at the German coast.

The backscattered radar signals from targets received by two antennas are processed separately into two complex images. Subsequently, these two complex images are combined into a single complex ATI or XTI image. The phase of the complex ATI image is proportional to the radial velocity (or motion toward the sensor) of ocean surface currents, and the phase of the complex XTI image is proportional to terrain height.

The accuracy of airborne interferometric acquisitions especially for coastal areas varies in the range of centimeters [1] to meters [2] for measurements of terrain heights and in the range of centimeters to decimeters per second for surface currents, [2]–[4]. Although it was stated that the separation of the XT- and AT-induced phase is difficult, due to the ambiguity in the combined interferometric phase, [5], a new approach of hybrid along- and cross-track interferometry is provided.

In this paper, a possible way of obtaining terrain heights and surface currents simultaneously by airborne interferometry is presented. For this purpose, a combined interferometric baseline with two antennas consisting of an along- and cross-track component is used. Afterward, a geometrical model for the interpretation of the interferometric phase is derived. We will focus especially on the derivation of surface currents from the combined interferometric phase. The obtained accuracies are in an order of 20 cms^{-1} and, thus, seem to be sufficient for coastal applications like sediment transport modeling or coastal engineering. Due to the highly dynamic character of Wadden Sea areas, a synoptic acquisition of morphology and surface currents in intertidal areas is of high value. This means that the data can be used for validation and assimilation in these models.

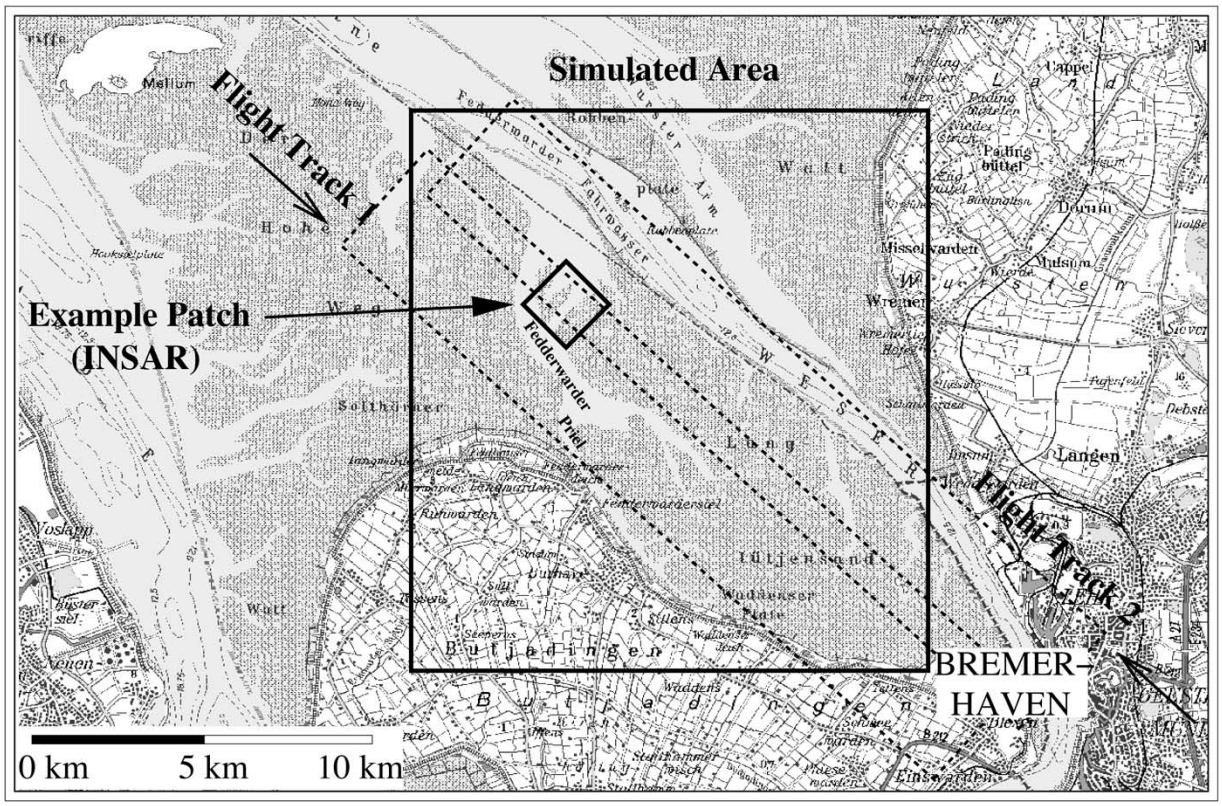

Fig. 1. Area of the experiment site located in the Weser Estuary.

The paper is organized as follows. First of all, the conditions during an experiment conducted in February 1997 are described. Depicted are the natural characteristics of the test site in the Wadden Sea, the flight conditions, and the radar configuration used for the experiment. Afterward, characteristics of the measured interferometric phase over water and land areas are presented. To derive the radial component of current velocity from the mixed phase, a new geometrical model for combined interferometric acquisitions is presented. To prove the theory, the model is applied to experimental data in the last section, and the results are compared to results from a hydrodynamic model.

II. Experimental Setup

On February 10, 1997, an airborne INSAR experiment was carried out over the Wadden Sea area of the German Bight, which is located at the estuary mouth of the Weser River at the German coast, near the city of Bremerhaven. Fig. 1 shows the Weser Estuary, the location of the experimental flight tracks and the coverage of the model area used as a reference.

The instrument used for acquisition was the interferometric SAR-system AeS-1. The radar operates at a center frequency of 9.55 GHz (X-band) with a bandwidth of 400 MHz, thus enabling the acquisition of SAR images with an optimum ground resolution of 0.5 m. Table I shows the main system parameters of the AeS-1.

The geometry of the AeS-1 is depicted in Fig. 2. Two antennas were mounted on the aircraft, forming a (cross-track) interferometric baseline of 1.56 m. At the same time, the baseline additionally had a small along-track component of 0.034 m. For acquisitions over Wadden Sea areas, the AeS-1 is flown at a mean height of 3200 m. With this flight setting, ambiguity heights of 35 m in midswath are obtained. Data of two antiparallel flight tracks are used for this study that overlap in a range of approximately 500 m, referred to as flight track 1 (T_1) and flight track 2 (T_2) (Fig. 1).

The Wadden Sea region itself consists of the shallow intertidal zone between land and the open sea that is periodically flooded during the tidal cycle. The mean tidal range is 3.6 m,

TABLE I
Radar Parameters for the Acquisition of T_1 and T_2

Operating frequency	9.55 GHz
System bandwidth	400 MHz
PRF	8 kHz
Polarization	HH
Pulse peak power	2.5 kW
Transmission/receiving modes	both antennas transmit - receive separately
Ground resolution	up to 0.5 m × 0.5 m
Swath width	4 km
Look angle at mid swath	45°
Flight velocity	84 ms^{-1} (T_1), 75 ms^{-1} (T_2)
Squint angle	9.7^o (T_1), −3.3^o (T_2)
Flight altitude	3200 m
InSAR baseline	0.034 m along track 1.56 m cross track

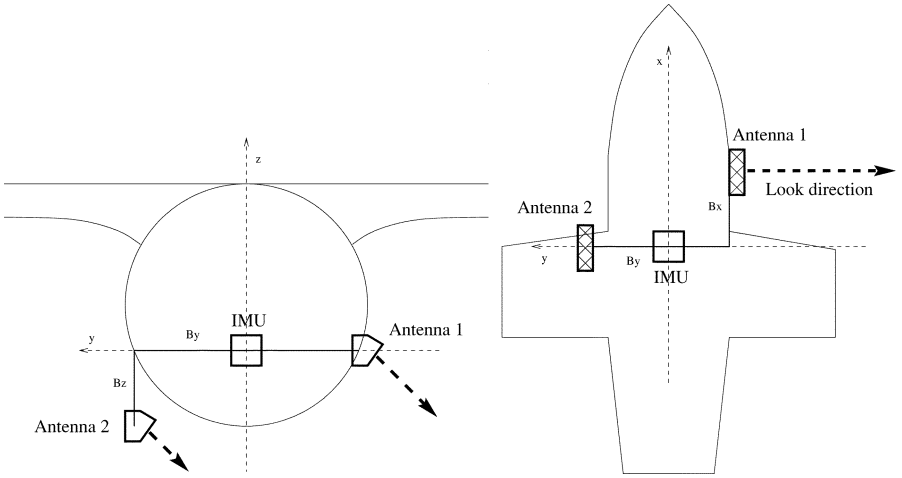

Fig. 2. Geometry of the interferometric Radar AeS-1.

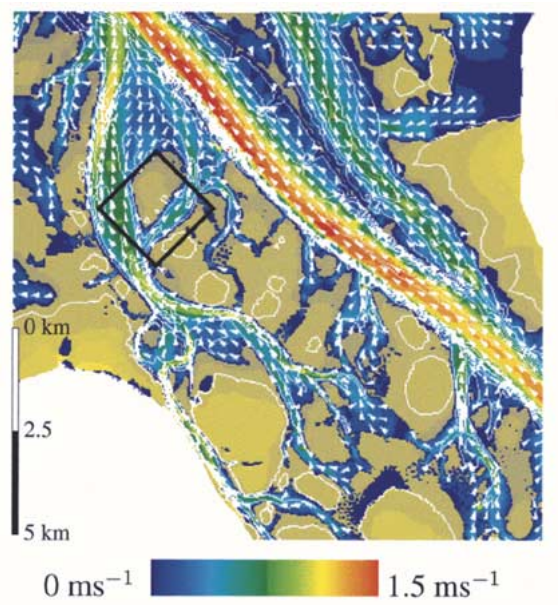

Fig. 3. Tidal currents as calculated by the model in the experimental area, 30 min before low tide. The box depicts the example area in the overlapping swaths.

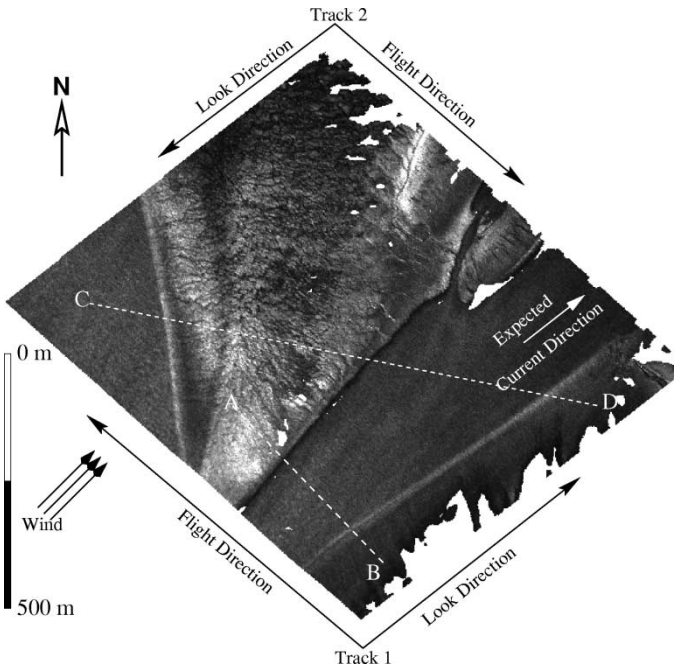

Fig. 4. Geocoded amplitude image of flight track T_1 with wind and expected current direction, as well as the flight geometry. The dashed lines depict the profile lines used for the discussion. The amplitude image covers an area of 1.2 km × 1.2 km.

which means that the characteristics of this area vary between totally flooded at high tide and partially fallen dry at low tide. The surface consists of tidal flats separated by tidal inlets and channels whose width ranges from 2–200 m. This tidal inlets canalize the tidal current, and most of them are flooded during the whole tidal cycle.

The acquisitions were conducted approximately half an hour before low tide. This means that a current in the tidal channels is flowing toward the open sea, i.e., from southwest to northeast in our test site. This tide situation is depicted in a resulting image of the hydrodynamic model TRIM-2D, which was provided by the Federal Waterway Engineering and Research Institute (Fig. 3). For illustration purposes, Fig. 4 depicts an amplitude image representing the according situation in our test area. Superimposed are the flight geometry, wind, and current directions. The magnitude of the maximum surface current velocity is expected to be in a range of 0.7–0.9 ms^{-1}. This date near to low tide was chosen due to the initial aims of this INSAR experiment, where a high-precision height model of the tidal flats had to be derived. Because of that, the nonflooded areas had to be mapped at its maximum extent at low tide.

Wind data were provided by the German Meteorological Office (Deutscher Wetterdienst) for the gauging station "Bremerhaven." The site is located directly at the coast, so that we consider a comparable wind field . The wind was rough and variable between 8–10 ms^{-1}, coming from southwest (see Fig. 4). These conditions lead to distortions of the flight attitude of the aircraft and, thus, of the antenna position. By measuring the aircraft motion using inertial measurement units (IMUs) and a differential global positioning system, the antenna geometry during the flight can be calculated. Due to the different wind angles at the two antiparallel tracks, a mean squint angle of 9.7° for flight track 1 and −3.3° for flight track 2 is obtained.

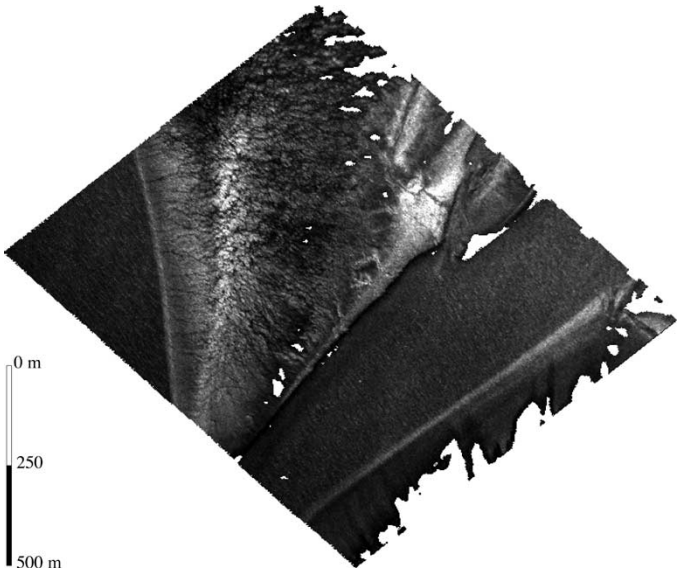

Fig. 5. Amplitude image of flight track T_2.

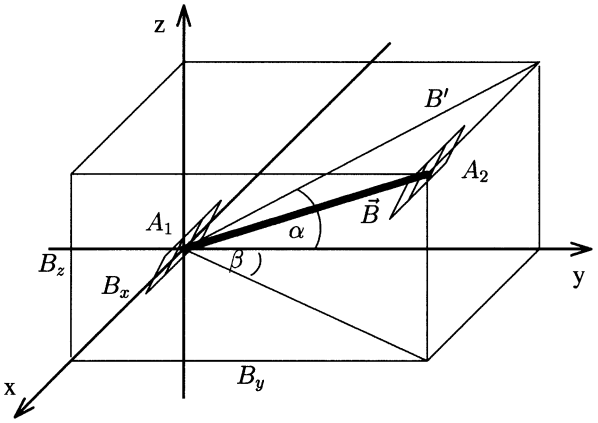

Fig. 6. Geometrical description of the mixed along- and cross-track baseline.

III. Theory for Hybrid Along and Cross Track Interferometry in Presence of Squint

A. Geometrical Model

In this section, the theoretical background for squinted interferometric imaging with along-track and cross-track baseline is presented. Fig. 6 illustrates the baseline configuration for a hybrid interferometric acquisition, while the imaging geometry of the radar system is depicted in Fig. 7. The two antennas A_1 and A_2 are mounted on the carrier platform (here the fuselage of an aircraft) separated by a baseline $\vec{B}$ with $\vec{B} = (B_x, B_y, B_z)$ in the x_0, y_0, and z_0 direction. Here, x_0 is the flight direction, y_0 and z_0 are in the plane perpendicular to x_0, and z_0 is in the vertical direction. The platform is considered to move constantly at a speed V parallel to x_0, which results in a time lag Δt between both antennas A_1 and A_2. Both antennas send and receive separately.

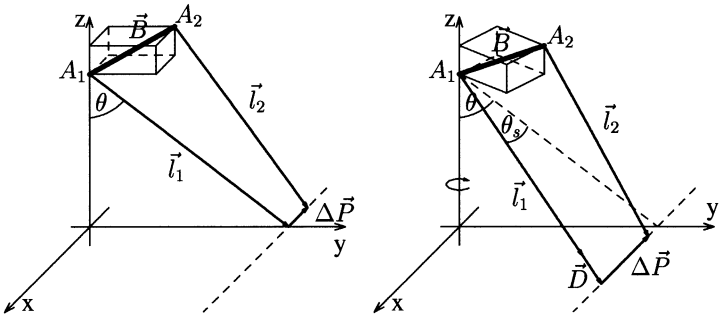

Fig. 7. Imaging geometry for hybrid interferometry with AT and XT component in presence of squint. (a) $\theta_s = 0$. (b) $\theta_2 \neq 0$.

The two vectors $\vec{l}_1$ and $\vec{l}_2$ represent the distance vector from A_1 and A_2 to a certain position on the surface at its closest approach [Fig. 7(a)]. $\Delta\vec{P}$ is then the distance vector on the surface parallel to x_0 between the two antennas and is given by $\Delta\vec{P} = (V\Delta t, 0, 0)$. In the "pure" cross-track case without squint, this distance is zero. In the "pure" along-track case, it is equal to the along-track baseline B_x.

As a target on the earth's surface moves at a velocity $\vec{U}$, this adds to the slant range distance, which can be expressed by the distance vector $\vec{D}$ given by $\vec{D} = \vec{U}\Delta t$. The distance vectors $\vec{l}_1$, $\vec{l}_2$ can be written in terms of the slant range distance R_1 from antenna 1 to the target as

$$\vec{l}_1 = (0, R_1 \sin\theta, -R_1 \cos\theta) \tag{1}$$

$$\vec{l}_2 = \vec{l}_1 - \vec{B} + \Delta\vec{P} + \vec{D}. \tag{2}$$

Here, θ denotes the look angle, as indicated in Fig. 7(a). The interferometric phase ϕ results from the range difference of $|\vec{l}_1|$ and $|\vec{l}_2|$, which can be expressed as

$$\phi = \frac{4\pi}{\lambda}\left(\sqrt{\langle\vec{l}_2, \vec{l}_2\rangle} - \sqrt{\langle\vec{l}_1, \vec{l}_1\rangle}\right) \tag{3}$$

where λ represents the wavelength, $\langle\vec{X}, \vec{Y}\rangle$ denotes the scalar product, and thus $|\vec{X}| = \sqrt{\langle\vec{X}, \vec{X}\rangle}$. After some basic vector operations and Taylor expansion, assuming $R_1 \gg |\vec{B}|$, the phase can be expressed as shown in (4)–(6) at the bottom of the page with

$$\langle\vec{l}_1, \vec{D}\rangle = R_1 U_r \Delta t$$

$$\langle\vec{l}_1, \vec{B}\rangle = R_1 B' \sin(\theta - \alpha)$$

$$B' = |(0, B_y, B_z)|.$$

$$\phi = \frac{4\pi}{\lambda}\left\{\sqrt{1 + \frac{2\langle\vec{l}_1, \vec{D}\rangle - 2\langle\vec{l}_1, \vec{B}\rangle + 2\langle\vec{l}_1, \Delta\vec{P}\rangle}{R_1^2} + \frac{|\vec{D}|^2 + |\vec{B}|^2 + |\Delta\vec{P}|^2}{R_1^2}} - 1\right\} R_1 \tag{4}$$

$$\approx \frac{4\pi}{\lambda R_1}\left\{\langle\vec{l}_1, \vec{D}\rangle - \langle\vec{l}_1, \vec{B}\rangle + \langle\vec{l}_1, \Delta\vec{P}\rangle\right\}, \qquad R_1 \gg |\vec{B}|, |\Delta\vec{P}|, |\vec{D}| \tag{5}$$

$$= \frac{4\pi}{\lambda}\left\{U_r \Delta t - B' \sin(\theta - \alpha)\right\} \tag{6}$$

Herein, α denotes the tilt angle of the baseline (see also Fig. 6). It should be added that the phase is dependent on the varying incidence angle θ_i over the whole swath width. This has to be considered in (6) so that the range-dependent interferometric phase ϕ_{int} results to $\phi_{\text{int}} = \phi \sin\theta_i$. The second term in (6) represents the cross-track and thus the topographic phase. Obviously, the topographic phase is changed by an additional motion-induced shift of $U_r \Delta t$, where Δt is the time lag that depends on the along-track baseline and the flight velocity.

To illustrate this, one can derive the formulas for the "pure" along- and cross-track phase analogous the derivation of the hybrid phase by setting either the cross-track component or the along-track component of the baseline to zero. Using (4), this results for $\vec{B} = (B_x, 0, 0)$ in the "pure" along-track phase relation as

$$\phi \approx \frac{4\pi}{\lambda R_1} \langle \vec{l}_1, \vec{D} \rangle \tag{7}$$

$$= \frac{4\pi}{\lambda} U_r \Delta t \tag{8}$$

$$= \frac{4\pi}{\lambda} B_x \frac{U_r}{V}. \tag{9}$$

Thus, surface velocities can be determined by calculating U_r. Otherwise, with $\vec{B} = (0, B_y, B_z)$, using (4), one obtains the "pure" cross-track phase and the resulting terrain heights

$$\phi \approx -\frac{4\pi}{\lambda} \langle \vec{l}_1, \vec{B}_1 \rangle \tag{10}$$

$$= -\frac{4\pi}{\lambda} |\vec{B}| \sin(\theta - \alpha). \tag{11}$$

Equation (6) indicates that the hybrid phase consists of the difference between the along- and cross-track phase, resulting in an ambiguity. For calculating the interferometric velocities, the topographic or cross-track component of the phase has to be removed. One way to determine the topographic phase is to use two interferometric measurements. While the topographic phase ϕ_{XT} remains constant, the along-track phase component ϕ_{AT} varies with look direction. As an example, two antiparallel flight tracks are used that are calibrated and geocoded. This means that the motion-induced phase changes its sign, so the phase of both tracks has to be subtracted in order for the topographic or cross-track phase to cancel. The hybrid phase of these tracks is then given as

$$\phi_1 = a_1 \phi_{AT} - b_1 \phi_{XT} \tag{12}$$

$$\phi_2 = -a_2 \phi_{AT} - b_2 \phi_{XT} \tag{13}$$

where a_i and b_i are constants.

In order to evaluate the phase, the phase component that is induced by the "flat earth" is given by

$$\phi_{\text{flat}} = \frac{4\phi}{\lambda} \left\{ U_r \Delta t - B' \left[\sin(\theta - \alpha) - \sin(\theta_0 - \alpha) \right] \right\}$$

$$= \frac{4\pi}{\lambda} \left\{ U_r \Delta t - \frac{B' \cos(\theta_0 - \alpha) H}{R_1 \sin\theta_0} \right\} \tag{14}$$

where H denotes the elevation of mapped area, and θ_0 is the start incidence angle in near range.

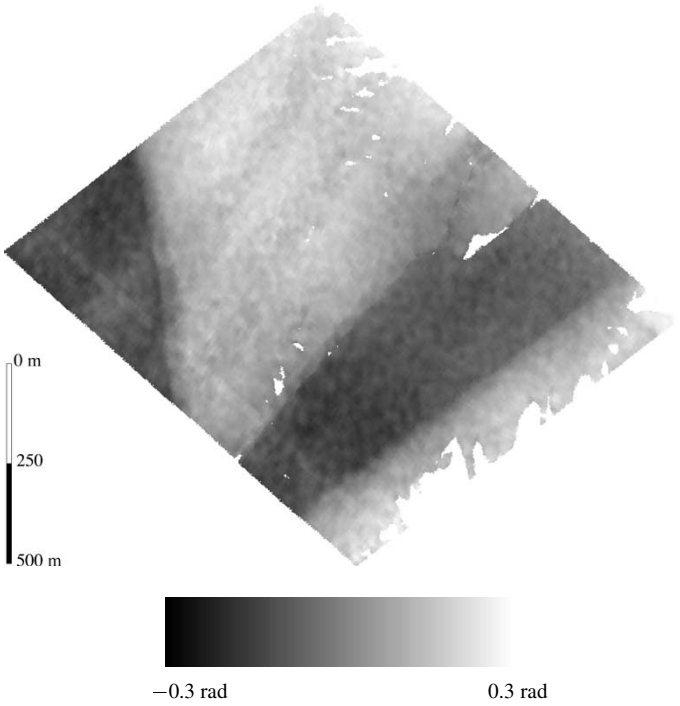

Fig. 8. Interferometric phase image of flight track T_1 derived by hybrid interferometric acquisition in an area of 1.2 km × 1.2 km.

B. Specific Properties of Hybrid Interferometry

The imaging of moving targets by a interferometric system with hybrid geometry results in a specific effect on the phase. Due to the radial velocity, the impulse response of the target is shifted in azimuth direction by a distance Δx [6]. Because the antennas are separated by a cross-track baseline, the range distances to the target vary by a difference ΔR. This results in different azimuth shifts of the two impulse response functions leading to a misregistration. The misregistration ΔX is given as

$$\Delta X = -\frac{\Delta R}{V} U_r. \tag{15}$$

This misregistration depends on the cross-track baseline and the radial velocity; thus, the amount of misregistration increases with increasing velocity of the target. Usually, one finds misregistration values in the range of centimeters for the conditions in our experiment.

Due to the squint angle θ_s, especially in airborne interferometry, the inexact coregistration results in an additional phase shift. This phase shift $\Delta\phi$ for squinted geometry was derived by [7] and is given as

$$\Delta\phi = \frac{4\pi}{\lambda} \Delta X (1 - \cos\theta_s). \tag{16}$$

This phase shift has to be considered in the derivation of the radial velocity. The effect can be minimized by using exact navigation data during the acquisition.

IV. Comparison With Experimental Data

Figs. 8 and 9 show the interferometric phase, where a phase shift over water surfaces in comparison to land areas is found. This can be interpreted as the phase change due to the motion of

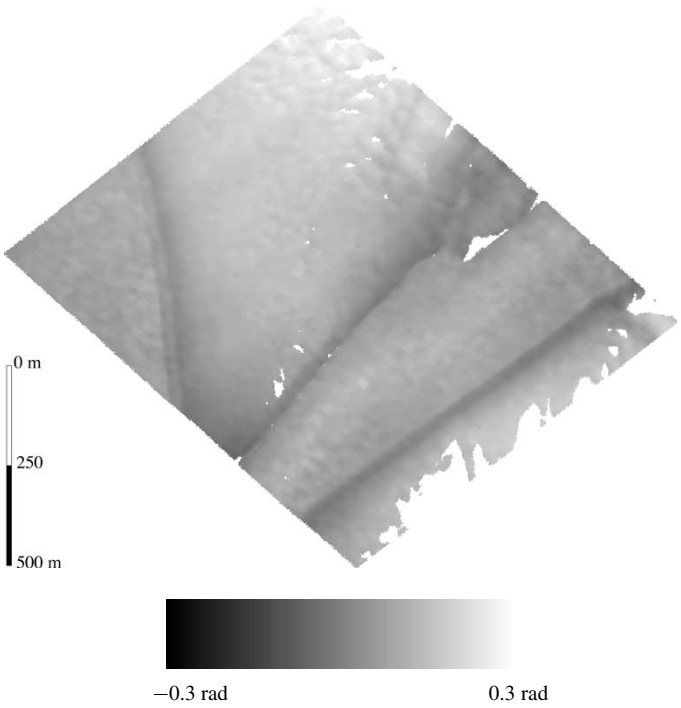

Fig. 9. Interferometric phase image of flight track T_2 derived by hybrid interferometric acquisition in an area of 1.2 km × 1.2 km.

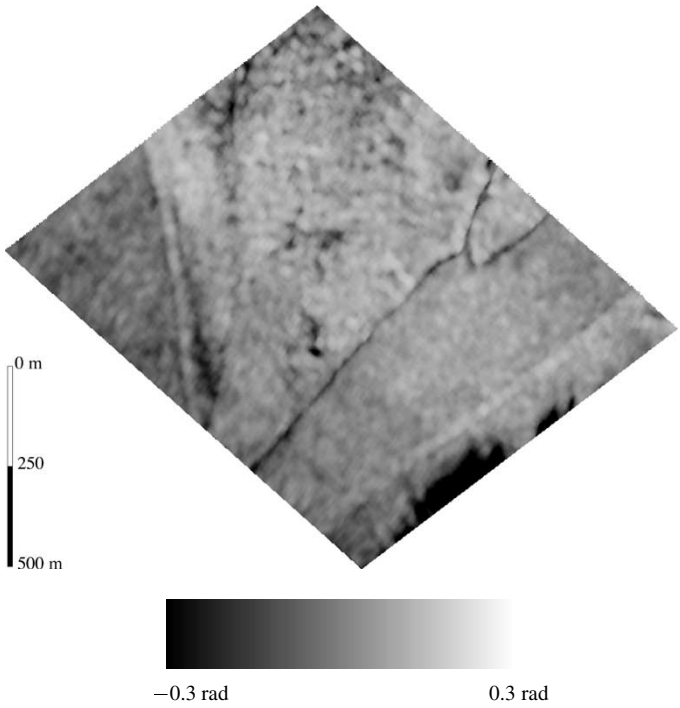

Fig. 10. Coherence image of flight track T_1.

the water surface. It is well known that with along-track interferometry, one is able to estimate the radial velocity of a scatterer and, thus, movements on the ocean surface [8]. The movement in the line of sight results in an interferometric phase shift, which is proportional to the radial velocity of the moving targets.

A. Interpretation of the Hybrid INSAR Phase

For further investigations of the interferometric phase data takes of two antiparallel flight tracks T_1 and T_2 covering the same area are evaluated jointly. For an overview of this area, the SAR amplitude images of both flights are given in Figs. 4 and 5. The imaged surface consists of a tidal channel to the western part and tributary stream spreading from southwest to northeast. The embedded tidal flats like the triangle-shaped region in the middle and the region at the southeast are smooth and nonflooded. The overlapping region of both acquisitions covers roughly $1.2 \times 1.2\,\mathrm{km}^2$. Due to the acquisition at two flight paths there is a time delay of 10 min between the acquisitions. Because the time interval is short, no significant change in the surface current inside the tidal channel is expected. According to the flight geometry, two important features can be observed.

First of all, the smaller tidal channel is parallel to the look direction. The water follows the main direction of the channel, and thus, a significant velocity component in range direction can be expected. According to the theory of along-track interferometric SAR (ATI) this results in a significant phase difference in the interferometric measurement. A second aspect is that the wind direction is southwest, and thus, it blows also parallel to the channel and the range direction (see Fig. 4).

Because the ATI determines the radial velocity which is a composed surface movement due to wind, phase velocity, and surface currents (neglecting orbital motion of longer waves), their contributions have to be separated. The influence of wind drift and the phase velocity of the Bragg waves on the ATI phase can be estimated according to [6]. In this case the effect of wind drift and Bragg wave phase velocity can be approximated linearly. A wind drag of 3% of the wind speed and a phase velocity component of approximately 22 cms^{-1} is assumed (valid for a Bragg wavelength of 1.7–3.1 cm at X-band, depending on the incidence angle), both in direction southwest to northeast.

Figs. 8 and 9 show the unwrapped and geocoded INSAR phase of T_1, T_2, and as an example the coherence image of T_1 (Fig. 10). The dependence on the incidence angle was corrected. The coherence is high also over water areas, so that a high degree of confidence for INSAR phase can be assumed. Generally, coherence values for acquisitions with the AeS-1 over the water surface are found in a range of 0.75–0.98. The phase statistics can then be calculated (see [9]). For the AeS-1 acquisition, this results in a phase standard deviation in a range of 0.005–0.02 rad. The phase noise leads then to a velocity variation of 0.03–0.07 ms^{-1} for the given geometry.

The profiles through the INSAR phase of T_1 and T_2 show the characteristic of the phase over water and land areas (Fig. 11). First of all, it is obvious that the motion-induced (ATI) phase is mapped with opposite sign according to the opposite look directions with respect to the direction of surface flow. In contrast to this, the phase over land (the cross-track INSAR (XTI) phase) remains unchanged. Thus, the tidal channel, in the profile of T_1, appears as deep, while, in the profile of T_2, rifts at the land–water boundary are apparent with an increasing phase over water: the phase value is higher than that of the surrounding tidal flat. This obviously cannot be interpreted as a topographic effect on the XTI phase but as the ATI component induced by the surface flow.

On the other hand, the phase over water areas is not uniformly distributed and follows a typical current profile for narrow channels. The distribution of the surface flow along the transects

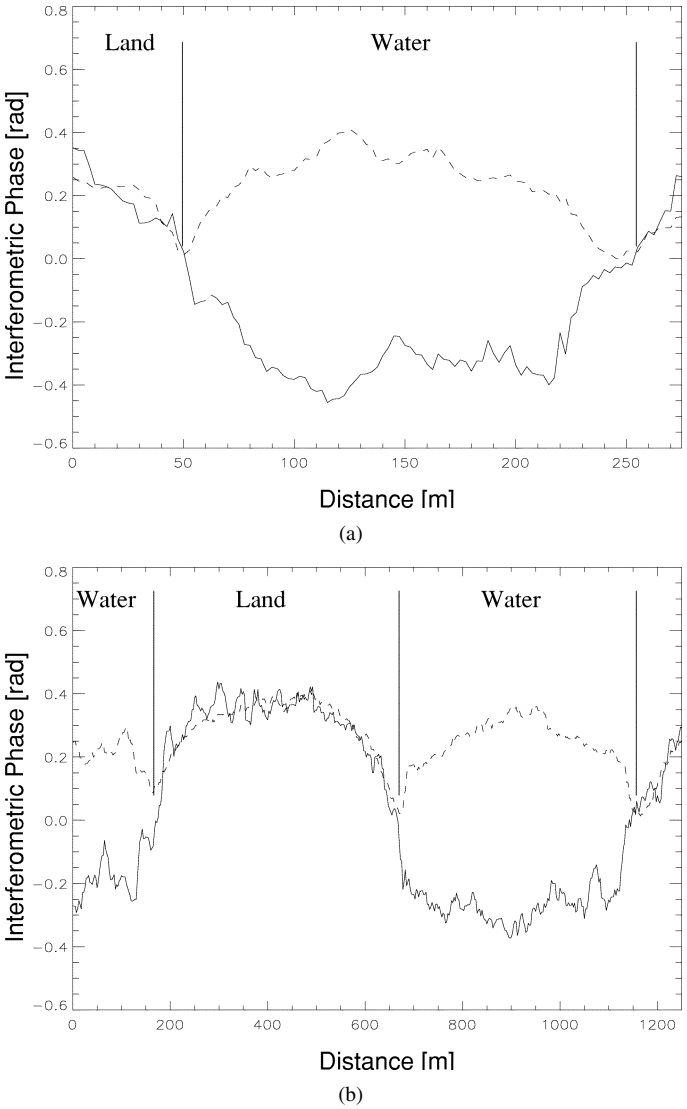

Fig. 11. (a) Profile 1 through the phase (A–B). (b) Profile 2 through the phase (C–D). Transects through the INSAR phase of T_1 and T_2. (Solid line) Track 1. (Dashed line) Track 2.

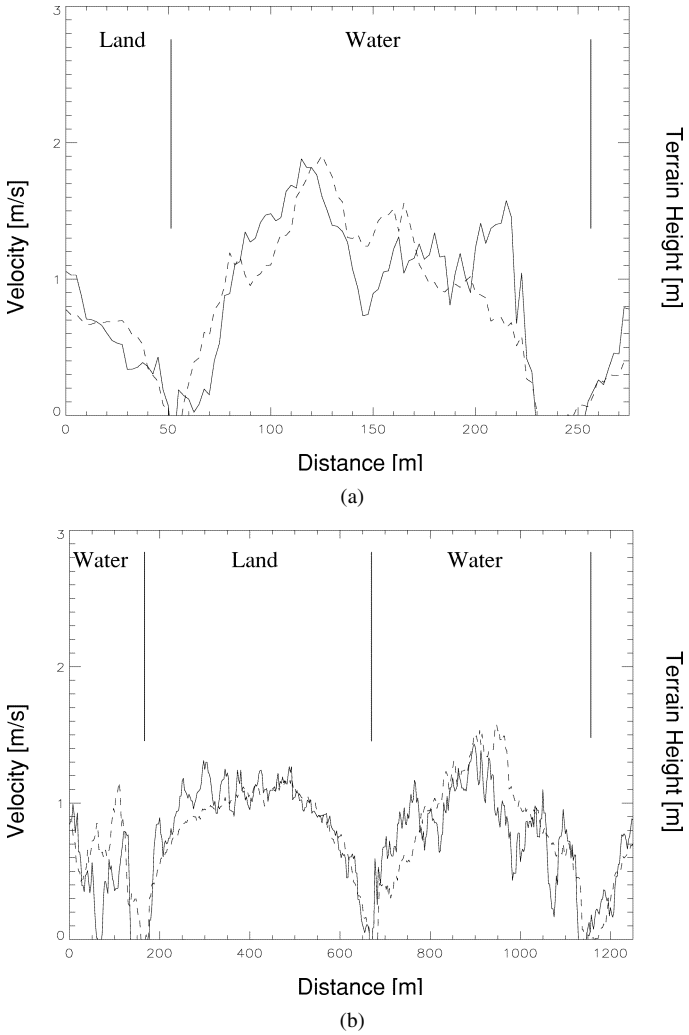

Fig. 12. (a) Profile 1 through the ground range velocity (A–B). (b) Profile 2 through the ground range velocity (C–D). Magnitude of the ground range radial velocities derived for profiles 1 and 2. (Solid line) Track 1. (Dashed line) Track 2.

show the opposite trend in the opposite track. Fig. 11 provides a good example for this. Following the profile (A-B) of T_2, over water the phase sets up at 0 rad and increases to a local maximum of 0.4 rad, decreasing afterward to a level of 0.2 rad and again to 0 rad at the land–water boundary. The transect through T_1 shows the inverted trend starting and ending with 0 rad at the land–water boundary decreasing to a local minimum of -0.4 and -0.25 rad in the surrounding level.

The same characteristic is true for the longer profile (C-D) (see Fig. 11). While the INSAR phase over land areas follows almost the same level in both tracks (discrepancies may occur due to radar systematic errors that are not explicitly corrected for), they spread up over water areas to values of 0.2–0.4 rad in T_2 and -0.4 to -0.2 in T_1.

B. Analysis

To analyze the hybrid ATI and XTI phase, the proposed model is applied, with the baseline vector $\vec{B} = (0.034, 0.682, -1.410 \text{ m})$ and squint angles between -3.3° and 9.6°. Regarding hybrid interferometry, the focus of this study is on the derivation of surface currents using the component of the along-track phase. The radial velocity in ground range projection can be determined by applying (6). The along-track phase difference is given by the relative phase difference between land and water, which is the difference between topographic-induced (XTI) phase and surface flow-induced (ATI) phase.

The results are compared by means of the phase profiles in Section IV-A. Equation (6) is used for the derivation of the ground range velocities. For comparison of the velocities, the ground range projection U_{rg} of the radial velocity U_r is used, in order to eliminate the dependence of the two datasets on the different incidence angle.

According to the phase profiles proposed in Section IV-A, Fig. 12 shows the ground range velocities derived with the along-track baseline of 0.034 m and flight velocities of 74.7 and 83.7 ms^{-1} for T_1 and T_2, respectively. The magnitude of the resulting velocities is in a range of up to a maximum value of 2 ms^{-1}. This maximum value seems to be overestimated in contrast to the mean velocities. To compete with this, an

influence of wind and the phase velocity of the Bragg waves has to be considered. Because wind drift and the phase velocity of the Bragg waves cause an additional velocity component to the estimated surface current, their effect has to be discussed. Therefore, the imaging geometry and the wind vector relative to the flight path are considered.

In this paper, a linear model for the ATI phase imaging is assumed. Nonlinear effects, as presented in the theory of [6], are expected to be marginal for an X-band radar due to the high incidence angle and the small R/V ratio (which is about 50 s in our case). For estimation of an existing bias in the along-track phase, only the hydrodynamic model is used, contrary to the investigation of [10], where *in situ* measurements using HF-radars were performed. Additionally, fully developed wind sea can be neglected due to the limited fetch.

Due to the rough wind of 8–10 ms^{-1}, it can be assumed that the propagation direction of the Bragg waves is parallel to the wind direction. Because the look direction and the wind direction are almost parallel, the phase speed and the wind drift are directed parallel to the look direction [6]. This means that that the wind direction is forward to the look direction in track 1 and against the look direction in track 2. Consequently, these components (0.3 ms^{-1} as 3% value of the windspeed for wind drift and 0.2 ms^{-1} phase velocity of the Bragg waves) follow the same direction as the current flow, so that the actual surface current velocity would be 0.5 ms^{-1} lower than the interferometric velocity, resulting in a total current of up to 1.5 ms^{-1}.

Considering the transect of T_1 (Fig. 12), the trend begins with 0 ms^{-1} at the land–water boundaries and increases up to 2 ms^{-1} and follows on to a level of 1.5 ms^{-1}. The velocity values of T_2 are similar but shifted by a small distance from T_1. The corresponding values in the velocity profile 2 are analogously distributed in a range from 0–2 ms^{-1}.

The ATI phase also provides the direction of the radial component, e.g., whether it is advancing or receding from the antenna. In our case, a negative phase shift indicates a flow away and a positive one toward the antenna. This means that the direction of the radial velocity component is parallel to the southwest–northeast direction (see Fig. 4), which is consistent with our expected current flow.

As an example, the resulting image of the simultaneous interferometric acquisition was added (Fig. 13). This shows the calculated terrain height and magnitude of the radial or interferometric velocities. The results of both tracks are calculated and averaged. Fig. 13 is, thus, a demonstration of combined measurement of terrain height over land and currents over water surfaces.

With a maximum of up to 2 ms^{-1}, the velocities seem to be overestimated. This results from the misregistration of the impulse response functions induced by the cross-track component and the movement of the scatterer (see Section III). The amount of misregistration grows with the radial velocity of the scatterer and with the increase of the squint angle. The distribution and the structure of the flow appears realistic. While the maximum is located in the middle of the channel, the velocities decrease toward the land–water boundary.

To give an estimate of the accuracy, the derived velocities of five areas in the channel are compared to the corresponding areas in the hydrodynamic model. The model results are calculated for a tide situation equivalent to the acquisition date of our interferometric data. Fig. 3 shows an overview of the model results in the whole estuary. The mean velocity of five areas on the water surface (Fig. 13) are regarded as an estimate of the velocity and the same areas in the hydrodynamic model as the reference. Table II shows the mean surface velocity and the surface current of the model.

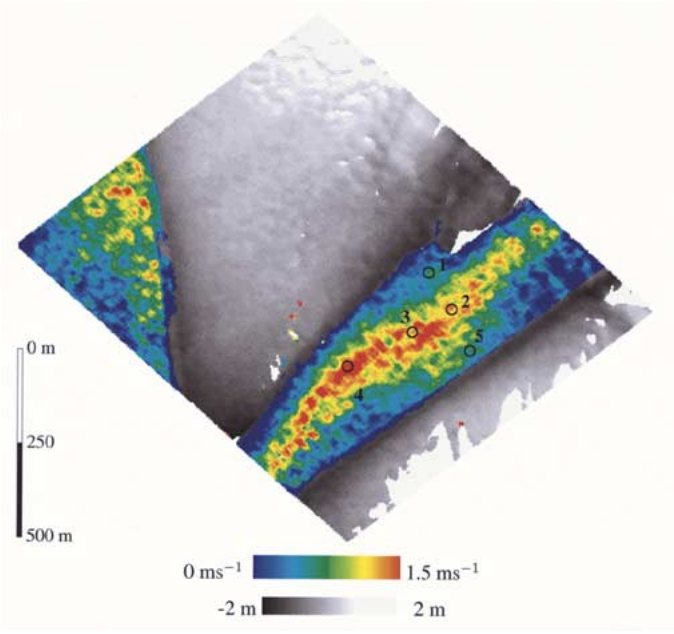

Fig. 13. Terrain height and ground range velocities obtained from T_1 and T_2.

TABLE II
INSAR-DERIVED SURFACE VELOCITIES AND MODEL RESULTS. $U_{\max} = 1.2\ \text{ms}^{-1}$ (MAXIMUM CURRENT VELOCITY IN THIS AREA. U_{30} = surface current velocity at low tide − 30 min

Testarea	1	2	3	4	5
INSAR [ms^{-1}]	0.6	0.8	1.0	1.3	0.7
Model U_{30} [ms^{-1}]	0.5	0.7	0.8	0.9	0.6
Difference [ms^{-1}]	0.1	0.1	0.2	0.4	0.1

The values of the surface velocity agree well for lower currents. The velocities differ in a range of up to 0.1 ms^{-1}. As the current speed increases, the difference increases. Deviations of up to 0.4 ms^{-1} indicate an error that increases with the velocity. This can be explained by the misregistration, as was pointed out in Section III. Using (15) and (16), the influence of misregistration can be estimated for the imaging geometry used in this paper. For a maximum velocity of 1.2 m/s, the misregistration (ΔX) is in a range of up to 2 cm. Considering the mean squint angles that were measured for the experimental data, one gets phase errors in a range of 0.02–0.1 rad. This results in corresponding velocities of 0.1–0.5 m/s, and finally, this agrees well with the observed overestimation of the interferometric derived velocity. Exact measurements of the surface velocity using this approach of hybrid interferometry need to account for misregistration and squint.

The results are promising for further use of INSAR measurements. The hybrid interferometry with along- and cross-track

components can provide a useful tool for coastal applications like model validation and current measurement. The maximum accuracy that can be achieved in terrain height and surface velocity is similar to "pure" cross-and along-track interferometry.

V. Conclusion

In this paper, the capability of hybrid along- and cross-track interferometry was shown for simultaneously estimating terrain height and surface currents by flying several flight tracks. Comparison of the new measurements with numerical model data leads to the following conclusions.

- The topographic data agree well with *in situ* measurements of the topography and can be optimized to a high-precision digital terrain model.
- The calculated surface currents agree with the currents, derived by the hydrodynamic model. The overestimation of the derived current velocity is caused by a phase offset that results from the squinted geometry.
- The time and space averaging carried out in the numerical hydrodynamic model has to be considered as one important error source in the comparison with the instantaneous data-take of the radar system.

The results are very promising for coastal applications. For further investigations and extended applications, some limitations have to be considered however, such as the following.

- Especially, flight planning has to consider that only the range-parallel component of the current field can be measured.
- The separation time between the acquisitions has to be short.
- A minimum windspeed is necessary; otherwise, a coherent imaging is not possible.
- Nonlinear effects associated with surface waves have to be taken into account in the general case.

This paper has shown that the following system requirements are of high importance for the proposed technique:

- accurate position and angular velocity data of the navigation system (this is the basic requirement in order to reduce systematic errors);
- radar hardware with a low phase noise and accurate known real baselines, as they are mounted on the aircrafts fuselage;
- accurate motion compensation technique in order to reduce systematic errors.

Although this is a first demonstration of the possibility to perform hybrid interferometry, the proposed technique gave very promising agreement with the available model data already. A more precise accuracy assessment of the terrain heights and surface currents derived by hybrid interferometry is currently in progress, e.g., using three antenna systems.

Acknowledgment

The authors would like to thank R. Schubert and N. Winkel (Federal Waterway Engineering and Research Institute (BAW) Hamburg), for their cooperation and for providing the model data.

References

[1] C. Wimmer, R. Siegmund, M. Schwäbisch, and J. Moreira, "Generation of high precision DEM's of the Wadden sea with airborne interferometric SAR," *IEEE Trans. Geosci. Remote Sensing*, vol. 38, pp. 2234–2245, Sept. 2000.

[2] H. Greidanus, E. Huising, Y. Platschorre, R. Van Bree, D. Van Halsema, and E. Vaessen, "Coastal currents with along track interferometry," in *Proc. IGARSS*, Hamburg, Germany, 1999, pp. 2607–2609.

[3] J. Campbell, A. Gray, J. Clarke, J. Gower, and K. Mattar, "Using the CCRS along track InSAR to measure and interpret ocean surface currents," in *Proc. IGARSS*, Lincoln, NE, 1996, pp. 1146–1148.

[4] L. Shemer, M. Marom, and D. Markman, "Estimates of currents in the nearshore ocean region using interferometric synthetic aperture radar," *J. Geophys. Res.*, vol. 98, no. C4, pp. 7001–7010, 1993.

[5] H. Greidanus, E. Huising, Y. Platschorre, R. Van Bree, D. Van Halsema, and E. Vaessen, "Coastal DEM's with cross track interferometry," in *Proc. IGARSS*, Hamburg, Germany, 1999, pp. 2161–2163.

[6] R. Romeiser and D. Thompson, "Numerical study on the along track interferometric radar imaging mechanism of oceanic surface currents," *IEEE Trans. Geosci. Remote Sensing*, vol. 38, pp. 446–458, Jan. 2000.

[7] M. Bara, R. Scheiber, A. Broquetas, and A. Moreira, "Interferometric SAR signal analysis in the presence of squint," *IEEE Trans. Geosci. Remote Sensing*, vol. 38, pp. 2164–2178, Sept. 2000.

[8] T. Ainsworth, S. Chubb, R. Fusina, R. Goldstein, R. Jansen, J.-S. Lee, and G. Valenzuela, "INSAR imagery of surface currents, wave fields and fronts," *IEEE Trans. Geosci. Remote Sensing*, vol. 33, pp. 1117–1123, Sept. 1995.

[9] D. Just and R. Bamler, "Phase statistics of interferograms with applications to synthetic aperture radar," *Appl. Opt.*, vol. 33, no. 20, pp. 4361–4368, July 1994.

[10] H. Graber, D. Thompson, and R. Carande, "Ocean surface features and currents measured with synthetic aperture radar interferometry and HF radar," *J. Geophys. Res.*, vol. 101, no. C11, pp. 25 813–25 832, 1996.

Robert Siegmund received the Diploma degree in geography from the University of Regensburg, Regensburg, Germany, in 1997. He is currently pursuing the Ph.D. degree and conducting his thesis in colaboration with the Coastal Research Laboratory, University of Kiel, Kiel, Germany.

Since 1997, he has been with Intermap Technologies GmbH (former Aero-Sensing Radarsysteme GmbH), Oberpfaffenhofen, Germany. His research work focuses on SAR interferometry and interferometric SAR data processing. This includes along- and cross-track interferometry and its application in coastal modeling.

Mingquan Bao, photograph and biography not available at the time of publication.

Susanne Lehner (M'01) received the M.S. degree in applied mathematics from Brunel University, Uxbridge, U.K., in 1979, and the Ph.D. degree in geophysics from the University of Hamburg, Hamburg, Germany, in 1984.

She was a Research Scientist with the Max-Planck Institute for Climatology, Hamburg, Germany, and in 1996, she joined the German Aerospace Center (DLR/DFD), Oberpfaffenhofen, Germany. She is currently a Research Scientist in the marine remote sensing at the Remote Sensing Technology Institute (DLR/IFM), working on the development of algorithms determining marine parameters from SAR.

Roberto Mayerle, photograph and biography not available at the time of publication.